Host–guest adaptability within oxothiomolybdenum wheels: structures, studies in solution and DFT calculations†‡

Jean-François Lemonnier,[a] Sébastien Floquet,*[a] Ali Kachmar,[b] Marie-Madeleine Rohmer,[b] Marc Bénard,[b] Jerôme Marrot,[a] Emmanuel Terazzi,[c] Claude Piguet[c] and Emmanuel Cadot*[a]

Received 13th March 2007, Accepted 27th April 2007
First published as an Advance Article on the web 24th May 2007
DOI: 10.1039/b703770h

The formation of host–guest cyclic architectures, built up through the self-condensation process of $[Mo_2O_2S_2]^{2+}$ oxothiocations around linear dicarboxylate ions such as adipate ($Adip^{2-}$), suberate (Sub^{2-}) and azelaate ($Azel^{2-}$) anions is reported. The complexes $[Mo_{12}Adip]^{2-}$, $[Mo_{12}Sub]^{2-}$ and $[Mo_{14}Azel]^{2-}$ have been characterized in the solid state by X-ray diffraction and in solution by ^{1}H NMR in different solvents (D_2O, DMF, DMSO and CD_3CN). The host–guest dynamics appear to be dependent on the nature of the system and are mainly governed by mutual adaptability between the host and the guest. ^{1}H NMR DOSY experiments show systematic differences, either positive or negative between the experimental and calculated molecular weights which appear to be correlated with the charge of the anion. The relative stabilities of the twelve-membered rings containing the $Adip^{2-}$, Pim^{2-} (pimelate) or Sub^{2-} anions were determined experimentally and decrease according to the order $[Mo_{12}Adip]^{2-} > [Mo_{12}Pim]^{2-} > [Mo_{12}Sub]^{2-}$. The host–guest adaptability depends on the length of the carbon chain and gives rise to selective encapsulation processes. Finally, theoretical DFT investigations in the gas phase yielded conformations whose symmetry and geometrical parameters proved consistent with X-ray structures and ^{1}H NMR spectra recorded in DMSO or DMF. Energy calculation highlights the high flexibility of the ring showing that only 3.1 kJ mol^{-1} accompanies the conformational change from circular to elliptical. The host–guest bond energy (ΔE) calculated for the Mo_{12}-based clusters is consistent with the experimental stability scale, major variations being due to some constraints undergone by the central alkyl chain.

Introduction

Polyoxometalates (POM) represent a wide family of inorganic compounds, which are of current interest for recognized applications in the fields of catalysis,[1–4] medicine,[5–7] magnetism,[8–12] analytical[13] or supramolecular chemistry.[9,14–21] In this context, polyoxothiometalates (POTM) emerge as a fascinating class of novel compounds which provides original transition metal ring-like clusters based on the self-condensation of $[M_2O_2S_2]^{2+}$ oxothiocations with M = Mo or W.[22,23] At variance with the standard structures of polyoxometalates, these compounds are characterized by a rare dynamic flexibility or host–guest self-adaptability, which are at the origin of a chemistry based on the *template synthesis* concepts. We showed that both the shape and the size of the Mo ring depend on the nature of the encapsulated species, such as phosphate, metalate or mono- and poly-carboxylate ions.[24–28] However, the synthesis of pre-designed nanoscale architectures with predictable nuclearity requires a fine control of the driving force which governs the formation of the host–guest assemblies. For instance, weak intramolecular interactions, such as π–π stacking or inner H-bond networks[29] increase the host–guest stability and lead to the formation of bis-templated rings. However, the presence of unsaturated carboxylate ions standing as embedded rigid pillars within the ring, prevents any dynamic behaviour.[29,30] Conversely, the use of flexible linear saturated alkyl dicarboxylate ions, results in highly flexible, distorted and fragile mono- or bis-templated rings.[26,27,31] Furthermore, the nuclearity of the resulting ring is directly related to the length of the alkyl chain. For instance, the use of oxalate (C2), glutarate (C5) and pimelate (C7) dianions led to 8-, 10- and 12-membered mono-templated rings, respectively.[26] However, some components of the series are missing and questions arise about the limits of the size that such host–guest systems could reach. Herein, we report a systematic investigation about the self-condensation properties of the $[Mo_2O_2S_2]$ building block around C6, C7, C8 and C9 dicarboxylate ions (see Scheme 1). Structural characterizations, dynamic and thermodynamic properties of dodeca- and tetradeca-molybdenum wheels obtained with these ligands are reported and discussed in relation to DFT calculations. Characterization of Mo_{12} and Mo_{14}

[a]*Institut Lavoisier de Versailles, UMR 8180, University of Versailles, 45 avenue des Etats Unis, 78035, Versailles, France. E-mail: sebastien.floquet@chimie.uvsq.fr, emmanuel.cadot@chimie.uvsq.fr*
[b]*Laboratoire de Chimie Quantique, Institut de Chimie-UMR 7177, CNRS-ULP, 4 rue Blaise Pascal, 67000, Strasbourg, France*
[c]*Department of Inorganic, Analytical and Applied Chemistry, University of Geneva, 30 quai E. Ansermet, CH-1211, Geneva 4, Switzerland*

† CCDC reference numbers 640033–640035. For crystallographic data in CIF or other electronic format see DOI: 10.1039/b703770h

‡ Electronic supplementary information (ESI) available: Selected bond lengths for $[Mo_{12}Adip]^{2-}$, $[Mo_{12}Sub]^{2-}$ and $[Mo_{14}Azel]^{2-}$ (Table S1); 300 MHz ^{1}H NMR spectra of $[Mo_{12}Adip]^{2-}$, $[Mo_{12}Pim]^{2-}$ and $[Mo_{12}Sub]^{2-}$ compared to those of uncoordinated $Adip^{2-}$, Pim^{2-} and Sub^{2-} in D_2O (Fig. S1); 300 MHz ^{1}H NMR spectra of $[Mo_{12}Adip]^{2-}$, $[Mo_{12}Pim]^{2-}$ and $[Mo_{12}Sub]^{2-}$ in DMSO-d_6 (Fig. S2); evolution of proportions of free Sub^{2-} and $[Mo_{12}Sub]^{2-}$ as a function of temperature in D_2O (Fig. S3). See DOI: 10.1039/b703770h

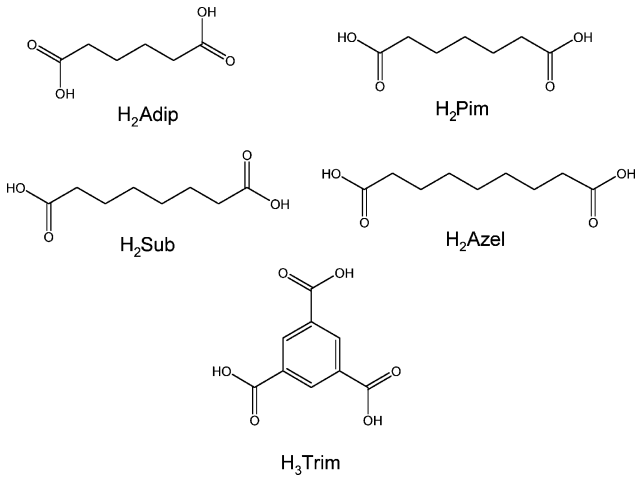

Scheme 1 Drawing of carboxylate ligands used in the present study.

wheels by ^{1}H diffusion ordered spectroscopy (DOSY method) is also reported. We present compiled DOSY data sets obtained from a larger series of templated oxothiomolybdate rings ranging from Mo_{12} to Mo_{16}. The systematic differences found between calculated and experimental molecular weights, extracted from DOSY experiments are discussed in relation to the solvation rate of the ring, depending on the ionic charge and on the size of the molybdenum clusters.

Results and discussion

Structures of the anions

The molecular structures of dodecamolybdenum rings, templated by adipate, pimelate and suberate anions are shown in Fig. 1a–c, respectively. The molecular representation of the $[Mo_{14}Azel]^{2-}$ anion is shown in Fig. 1d. Crystal data are given in Table 1 and selected bond lengths are listed in Table S1 (ESI‡). A basic description of the molecular architectures consists of a single guest dicarboxylate anion encapsulated in a cyclic inorganic neutral skeleton $[Mo_{2n}S_{2n}O_{2n}(OH)_{2n}]$ with $n = 6$ or 7. The $[Mo_2S_2O_2]^{2+}$ building blocks are connected through double hydroxo bridging ligands, which span non-bonding Mo–Mo contacts (3.223(1)–3.410(1)Å) alternating with short Mo–Mo bonding contacts within the building blocks (2.792(1)–2.849(1) Å).

$[Mo_{12}O_{12}S_{12}(OH)_{12}(H_2O)(C_6H_8O_4)]^{2-}$, $[Mo_{12}Adip]^{2-}$. The dodecamolybdenum wheel $[Mo_{12}Adip]^{2-}$ consists of six $[Mo_2S_2O_2]^{2+}$ fragments assembled around an adipate ligand (Fig. 1a) with C_s symmetry in the solid state. The two carboxylate groups of $Adip^{2-}$ are asymmetrically anchored to the inorganic host. For one carboxylate group (O19–C1–O20), oxygen O19 contracts a single bond with Mo1, while O20 bridges Mo2 and Mo3. The opposite carboxylate group (O21–C6–O22) is connected to Mo7 and Mo8 through two single bonds, respectively. The coordination bond distances between carboxylate groups and Mo atoms are in the

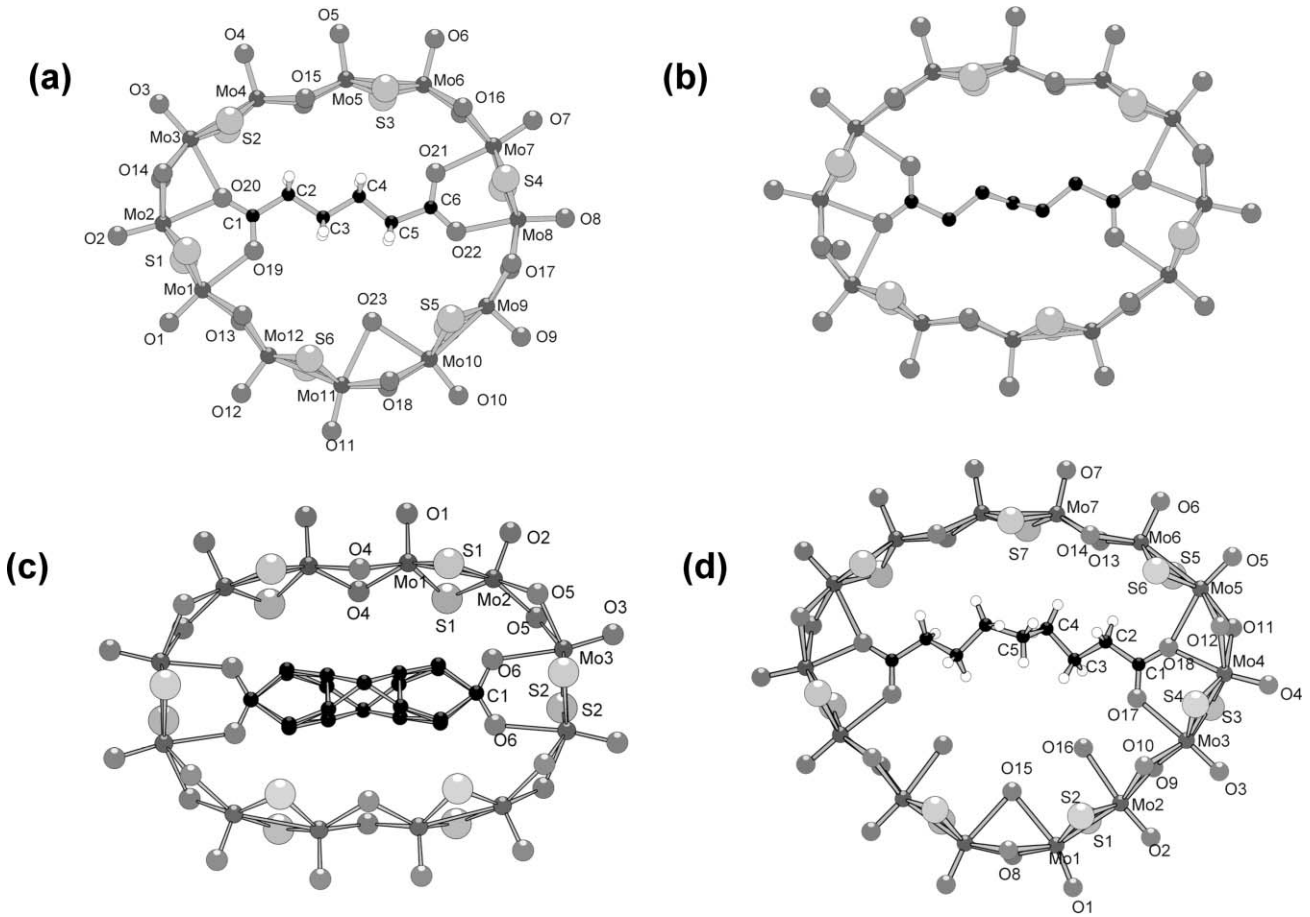

Fig. 1 Labelled molecular structures of the complexes $[Mo_{12}Adip]^{2-}$ (a), $[Mo_{12}Pim]^{2-}$ (from ref. 26) (b), $[Mo_{12}Sub]^{2-}$ (c) and $[Mo_{14}Azel]^{2-}$ (d).

Table 1 Structural parameters for compounds $(NMe_4)_2[Mo_{12}Adip]$, $K_2[Mo_{12}Sub]$ and $(NMe_4)_2[Mo_{14}Azel]$

Compound	$(NMe_4)_2[Mo_{12}Adip]$	$K_2[Mo_{12}Sub]$	$(NMe_4)_2[Mo_{14}Azel]$
Empirical formula	$C_{14}H_{104}Mo_{12}N_2O_{58}S_{12}$	$C_8K_2Mo_{12}O_{56}S_{12}$	$C_{17}H_{88}Mo_{14}N_2O_{60}S_{14}$
Formula weight	2764.99	2606.28	3022.49
T/K	100(2)	293(2)	293(2) K
Crystal size/mm	0.30 × 0.20 × 0.04	0.24 × 0.20 × 0.12	0.40 × 0.30 × 0.24
Crystal system	Orthorhombic	Tetragonal	Monoclinic
Space group	*Pnma*	$P4_2/mnm$	$C2/c$
a/Å	24.755(2)	18.4395(4)	13.0709(3)
b/Å	11.3210(6)	18.4395(4)	27.1242(5)
c/Å	30.229(2)	11.5430(6	30.5257(6)
α/°	90	90	90
β/°	90	90	97.899(1)
γ/°	90	90	90
V/Å^3	8471.5(8)	3924.8(2)	10719.8(4)
Z	4	2	4
D_c/g cm^{-3}	2.168	2.205	1.873
μ/mm^{-1}	2.103	2.364	1.928
Data/restraints/parameters	12926/0/518	3122/8/122	15730/8/523
R_{int}	0.0591	0.0357	0.0297
Final R indices [$I > 2\sigma(I)$]	$R_1 = 0.0427$, $wR_2 = 0.1191$	$R_1 = 0.0333$, $wR_2 = 0.0988$	$R_1 = 0.0483$, $wR_2 = 0.1359$

usual range (2.272–2.418 Å). The volume left inside the Mo_{12} cavity by the C6 adipate ion is filled by a water molecule bridging the Mo10 and Mo11 atoms through long bonds (2.471(5)–2.542(5) Å). Consequently, seven Mo atoms display octahedral environments, while the other five exhibit square pyramidal geometries.

Solvation of $[Mo_{12}Adip]^{2-}$ in the solid state. The structure of the $[Mo_{12}Adip]^{2-}$ anion reveals that the hydration sphere contains 22 water molecules equally distributed over both sides of the ring (see Fig. 2). The cohesion of the solvation sphere of the ring is ensured through H-bonds and occurs on specific solvation sites distributed as H-donor or H-acceptor sites. On each side, 6 water molecules are located in the vicinity of the 6 hydroxo bridges and display O···O distances distributed over a narrow range [2.69 ± 0.02 Å], characteristic of strong H-bonds. These water molecules are H-bound to five additional water molecules [O···O = 2.79–3.15 Å] mutually interacting through H-bonds [O···O = 2.76–2.94 Å], which leads to a pair of distorted hexagonal-like clusters of 11 water molecules each capping both sides of the $[Mo_{12}Adip]^{2-}$ anion.

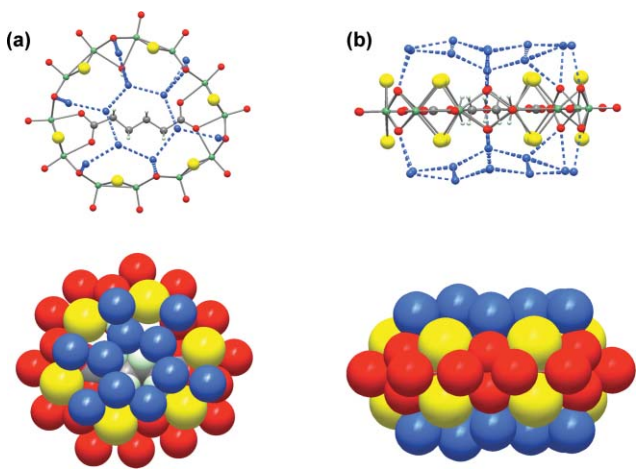

Fig. 2 Top (a) and side views (b) of the first hydration sphere of $[Mo_{12}Adip]^{2-}$ in the solid state (top: ball-and-stick models, bottom: space filling models,). The balls represent the water molecules (blue), the oxygen atoms belonging to the ring (red), the sulfur atoms (yellow), the molybdenum atoms (green) and the carbon atoms (grey).

$[Mo_{12}O_{12}S_{12}(OH)_{12}(C_8H_{12}O_4)]^{2-}$, $[Mo_{12}Sub]^{2-}$. The molecular structure of the $[Mo_{12}Sub]^{2-}$ ion (Fig. 1c) consists of a D_{2h} cyclic arrangement containing a highly disordered C8 alkyl chain. Despite various attempts to obtain defined locations for the six central carbon atoms, i) by downgrading from $P4_2/nmn$ to $P\bar{1}$ the symmetry of the space group in which the structure was solved, ii) by collecting X-ray data at low temperature (100 K), iii) by recording other crystals differing in the nature of the counter cations, iv) by changing the conditions of crystallization, or v) by introducing constraints for the C–C bond lengths and the C–C–C or O–C–C angles within the Sub^{2-} anion, the central disorder of the template always remains, as an intrinsic feature of the $[Mo_{12}Sub]^{2-}$ anion. However, the location of both carboxylate ends appears well defined inside the wheel. The disordered carbon atoms are distributed along a defined pathway running out of the mean plane defined by the 12 Mo atoms and drawing the contours of the conformational arrangement of the alkyl chain (see Fig. 1c). DFT calculations carried out on $[Mo_{12}Sub]^{2-}$ optimized in the gas phase revealed that a suberate alkyl chain constrained to fit into a dodecamolybdate ring can adopt several conformations, which fall in a narrow energy range. For each of them, the folded alkyl chain displays an out-of-plane displacement by about 2.1 Å, which is characteristic of substantial distortions within the Mo_{12} cavity (see below, DFT calculations). Finally, no water molecule was found and eight Mo atoms adopt a square pyramidal arrangement, whereas the other four are octahedral.

$[Mo_{14}O_{14}S_{14}(OH)_{14}(OH_2)_3(C_9H_{14}O_4)]^{2-}$, $[Mo_{14}Azel]^{2-}$. The $[Mo_{14}Azel]^{2-}$ anion depicted in Fig. 1d consists of a Mo_{14}-ring which adopts a characteristic *heart*-shape with idealized C_{2v} symmetry. In constrast to $[Mo_{12}Sub]^{2-}$, the alkyl chain of the azelaate anion is well defined with only the central C5 atom disordered between two positions. The azelaate anion is symmetrically anchored in the hemicycle of the cavity defined by

the five Mo atoms labeled from Mo3 to Mo7 and their symmetric counterparts, while the part spanning Mo1 and Mo2 is lined by three water molecules. Two of them (O16) appear singly bound to the Mo2 atoms, the third one (O15) bridging both equivalent Mo1 atoms, with the long Mo–O distances (2.461(3)–2.566(3) Å) characteristic of Mo–OH_2 bonds.

NMR studies in solution

The ^{1}H NMR spectra of compounds $[Mo_{12}Adip]^{2-}$, $[Mo_{12}Sub]^{2-}$ and $[Mo_{14}Azel]^{2-}$ were recorded either at room temperature or at variable temperature in D_2O, DMSO, DMF and in CD_3CN. Selected data and spectra are reported in Table 2, Fig. 3–7 and Fig. S1 and S2 (ESI‡).

$[Mo_{12}O_{12}S_{12}(OH)_{12}(H_2O)(C_6H_8O_4)]^{2-}$, $[Mo_{12}Adip]^{2-}$. In D_2O, the ^{1}H NMR spectrum of $[Mo_{12}Adip]^{2-}$ appears quite independent of the temperature between 275 and 350 K. At 300 K, it consists of twin broad signals ($\Delta\nu_{1/2} = 20$–25 Hz, non-resolved triplet) centred at −0.79 and −0.71 ppm, assigned to the methylene protons of the encapsulated $Adip^{2-}$ guest (Fig. S1, ESI‡). As a fingerprint of the guest encapsulation, these protons are significantly shielded with respect to those of the free $Adip^{2-}$ anion (2.13 ppm and 1.48 ppm).[26,29] Three additional peaks assigned to the DMF solvate in $Cs_2[Mo_{12}Adip]\cdot 7DMF\cdot 11H_2O$ are observed at 7.82, 2.90 and 2.75 ppm. In DMF-d_7 (or in DMSO-D_6), at room temperature (Fig. 3a and Fig. S2a,‡ respectively), the spectrum of $[Mo_{12}Adip]^{2-}$ consists of four NMR signals, distributed between two distinct spectral domains. In DMF-d_7, at 300 K, the chemical shifts of the

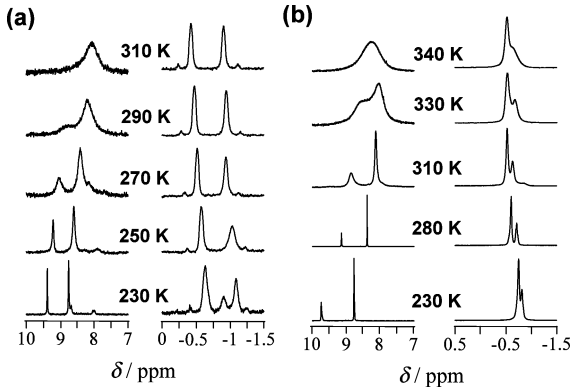

Fig. 4 Variable temperature 300 MHz ^{1}H NMR spectra of $[Mo_{12}Adip]^{2-}$ (a) and $[Mo_{12}Sub]^{2-}$ (b) in CD_3CN.

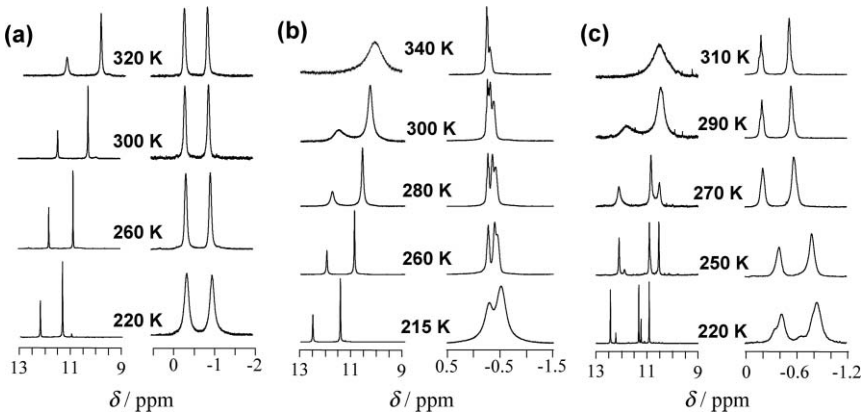

Fig. 3 Variable temperature 300 MHz ^{1}H NMR spectra of $[Mo_{12}Adip]^{2-}$ (a), $[Mo_{12}Sub]^{2-}$ (b) and $[Mo_{12}Pim]^{2-}$ (c) in DMF-d_7.

Table 2 Selected NMR data recorded at laboratory temperature

Compound	Solvent	δ (ppm) (Integration)
$Adip^{2-}$	D_2O	2.13 (4H); 1.48 (4H)
$[Mo_{12}Adip]^{2-}$	D_2O	−0.71 (4H); −0.79 (4H)
$[Mo_{12}Adip]^{2-}$	DMSO	11.29 (4H); 10.37 (8H); −0.65 (4H); −1.16 (4H)
$[Mo_{12}Adip]^{2-}$	DMF	11.45 (4H); 10.26 (8H); −0.33 (4H); −0.91 (4H)
$[Mo_{12}Adip]^{2-}$	CD_3CN	8.01 (12H); −0.41 (4H); −0.89 (4H)
Pim^{2-}	D_2O	2.44 (4H), 1.80 (4H), 1.56 (2H)
$[Mo_{12}Pim]^{2-}$	D_2O	−0.20 (4H); −0.53 (6H)
$[Mo_{12}Pim]^{2-}$	DMSO	11.45 (4H); 10.27 (8H); −0.71 (4H); −0.98 (6H)
$[Mo_{12}Pim]^{2-}$	DMF	11.40 (4H); 10.40 (8H); −0.19 (4H); −0.53 (6H)
$[Mo_{12}Pim]^{2-}$	CD_3CN^a	8.45 (12H); −0.49 (4H); −0.79 (2H); −0.90 (4H)
Sub^{2-}	D_2O	2.12 (4H); 1.45 (4H); 1.21 (4H)
$[Mo_{12}Sub]^{2-}$	D_2O	−0.26 (mult.); −0.65 (mult.) −0.75 (mult.)
$[Mo_{12}Sub]^{2-}$	DMSO	−0.85 (m); −0.77 (m); 10.23 (s); 11.21 (s)
$[Mo_{12}Sub]^{2-}$	DMF	11.55 (4H); 10.33 (8H); −0.30 (12H)
$[Mo_{12}Sub]^{2-}$	CD_3CN	8.96 (4H); 8.21 (8H); −0.55; −0.66
$Azel^{2-}$	D_2O	2.12 (4H), 1.45 (4H); 1.20 (6H)
$[Mo_{12}Azel]^{2-}$	D_2O	−0.38 (8H); −0.68 (6H)
$[Mo_{12}Azel]^{2-}$	CD_3CN	9.32 (4H); 9.25 (sh., 2H); 8.46 (4H); 8.19 (4H); −0.35 (mult.); −0.59 (mult.); −0.75 (mult.)

[a] $T = 316$ K.[26]

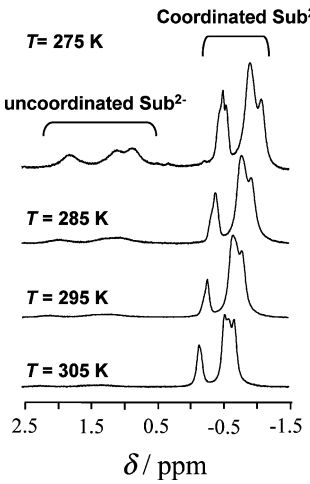

Fig. 5 Variable temperature 300 MHz ^{1}H NMR spectra of $[Mo_{12}Sub]^{2-}$ in D_2O.

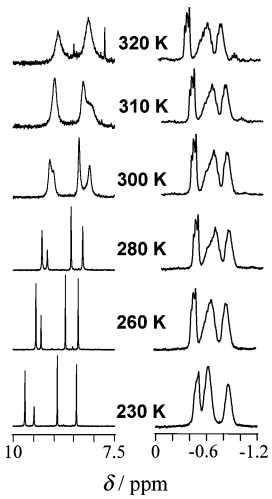

Fig. 6 Variable temperature 300 MHz ^{1}H NMR spectra of $[Mo_{14}Azel]^{2-}$ in CD_3CN.

two equal resonances corresponding to the methylene group are displaced at −0.33 and −0.91 ppm while two sharp lines at 11.45 and 10.26 ppm with 1 : 2 intensity ratio are assigned to the hydroxo bridges, observed because of the slow H–D exchange process. The variable temperature ^{1}H NMR experiments carried out in DMF-d_7 in the 215–350 K range (Fig. 3a) show that the features of the spectrum are maintained over the complete temperature range. Nevertheless, from $T = 215$ to $T = 340$ K, the hydroxo resonances gradually broadened from 6–7 Hz to 70–80 Hz, and shifted toward low frequencies, while the methylene signals remain almost unchanged. The ^{1}H NMR pattern is consistent with an averaged conformation of the host–guest system, rather close to D_{2h} symmetry (instead of C_s in the solid state). The D_{2h} arrangement imposes a symmetric anchoring of the adipate ion within the molybdenum ring, associated with the release (or the fast exchange) of the attached water molecule (see Fig. 1a). DFT calculations (see below) provide a C_{2h} structural model, very close to the D_{2h} formal symmetry (see Fig. 8a), which could be viewed as a limiting conformation, averaged to D_{2h} through slight fluxional dynamics occurring in solution. The D_{2h}-averaged symmetry is maintained over the temperature scale ($T = 220$–320 K), and it is consistent with an adipate ion strongly anchored at the centre of the cavity. The hopping of the carboxylate groups could be hindered by solvent molecules like water, DMF or DMSO, able to coordinate the inner molybdenum sites available for bonding. The broadening of the hydroxo signals with temperature is a common feature, explained by a fast exchange (inter-molecular exchange) with protons originating in uncoordinated water. The shielding effect observed for the hydroxo group ($\Delta\delta = 1.1$ and 1.7 ppm, respectively) as temperature increases, can be explained either by a temperature-dependent solvation rate of the ring, or by proton fast exchange. Beyond 340 K in DMF (or in DMSO), the $[Mo_{12}Adip]^{2-}$ anion irreversibly decomposes to give uncoordinated adipate ion and unknown Mo-containing species.

The ^{1}H NMR spectra recorded in CD_3CN as a function of the temperature are depicted in Fig. 4a. In this solvent, the dynamics of $[Mo_{12}Adip]^{2-}$ appears quite similar. At $T = 310$ K, the single broad resonance attributed to the hydroxo groups corresponds to proton fast exchange. When the temperature decreases, two NMR lines with 1 : 2 intensities characteristic of the averaged D_{2h} symmetry appear and sharpen until 5–6 Hz at 230 K. Concurrently, below $T = 270$ K, a new set of weak resonances with equal intensities is observed, distributed as three lines in the domain of the hydroxo resonances (8.68, 8.03 and 7.99 ppm for $T = 230$ K) and two lines in the methylene region at −0.91 and around −0.64 ppm (on the basis of its intensity, the −0.64 ppm line contains two components belonging to D_{2h} and C_{2h} conformers). These lines are characteristic of a new frozen conformation for $[Mo_{12}Adip]^{2-}$ and are consistent with the C_{2h} limiting conformation suggested by the DFT calculations. The quantity of the C_{2h} conformer represents about 15% at $T = 230$ K. To summarize, the $[Mo_{12}Adip]^{2-}$ anion in CD_3CN displays a D_{2h} averaged conformation at room temperature, which gives rise to a frozen C_{2h} conformation at low temperature. Conformational variation does not involve any carboxylate hopping since no significant change with temperature is observed in the methylene region, but then probably results from a slight fluxional dynamic.

$[Mo_{12}O_{12}S_{12}(OH)_{12}(C_8H_{12}O_4)]^{2-}$, $[Mo_{12}Sub]^{2-}$. The ^{1}H NMR spectrum of $[Mo_{12}Sub]^{2-}$ in D_2O consists of three broad signals (unresolved triplets) centred at −0.26, −0.65 and −0.75 ppm, corresponding to a Sub^{2-} anion coordinated inside the molybdenum ring (Fig. S1, ESI‡). A variable temperature experiment carried out in D_2O between 275 K and 305 K (see Fig. 5) reveals growing signals assigned to uncoordinated suberate ions (three equal signals at 2.12, 1.45 and 1.21 ppm), which gradually increase as the temperature decreases. The release of free suberate anions suggests that equilibrium (1) takes place.

$$[Mo_{12}Sub]^{2-} + 6\ H_2O \rightleftarrows [Mo_{12}(H_2O)_6] + Sub^{2-},\ K_{eq} \qquad (1)$$

From the integrated signals of uncoordinated Sub^{2-} and $[Mo_{12}Sub]^{2-}$, standard thermodynamic parameters ΔH_R and ΔS_R, are derived and give $\Delta H_R = -60.2$ kJ mol^{-1} and $\Delta S_R = -297$ J mol^{-1} K^{-1} (see Fig. S3, ESI‡), indicating that the encapsulation process of the template is driven by entropy.[27]

In DMF-d_7, the spectrum of $[Mo_{12}Sub]^{2-}$ exhibits a close set of unresolved lines centred at about −0.30 ppm corresponding to the resonances of the twelve methylene protons of the alkyl chain and of two single resonances at 11.55 and 10.33 ppm attributed to the

hydroxo bridges of the inorganic moiety (see Fig. 3b). The relative intensity of the separated signals (3 : 2 : 1, respectively) fully agrees with the expected formula $[Mo_{12}O_{12}S_{12}(OH)_{12}(C_8H_{12}O_4)]^{2-}$ in a D_{2h} symmetry.

Variable temperature experiments of $[Mo_{12}Sub]^{2-}$ in DMF-d_7, recorded between 350 K and 215 K reveal (i) an irreversible degradation of $[Mo_{12}Sub]^{2-}$ above 340 K, (ii) a fast exchange of protons at 340 K and (iii) a single D_{2h} conformation, observed below 340 K. The D_{2h} symmetry in solution is readily related to that determined in the solid state (see Fig. 1c). The behaviour of $[Mo_{12}Sub]^{2-}$ either in DMF or in CD_3CN (Fig. 3b and 4b) parallels that observed for $[Mo_{12}Adip]^{2-}$. No host–guest dynamic effect (apart from the proton fast exchange) is readily detectable on the NMR time scale. Such a behaviour is ascribed to steric constraints occurring between the Mo_{12}-ring and the C8 linear dicarboxylate ion, which hinder any facile hopping for the carboxylate groups over the adjacent coordination sites.

$[Mo_{12}O_{12}S_{12}(OH)_{12}(C_7H_{10}O_4)]^{2-}$, $[Mo_{12}Pim]^{2-}$. The dynamic behaviour of this compound was previously reported in CD_3CN between 296 and 226 K.[26] At low temperature, two frozen C_{2h} and D_{2h} conformations were observed for $[Mo_{12}Pim]^{2-}$ in a 2 : 1 ratio, respectively. A similar pattern is obtained in DMF-d_7 (see Fig. 3c). At 270 K, the three lines observed for the hydroxo resonances and the two signals of the methylene protons with 2 : 2 : 2 : 2 : 3 relative intensities are consistent with an averaged C_{2h} symmetry for the host–guest system. At lower temperature (T = 220 K), two additional signals arise in both resonance regions. The multiplicity and the intensity ratio allow an assignment of these signals to a D_{2h} frozen conformation. As observed in CD_3CN, the ^{1}H NMR spectrum of $[Mo_{12}Pim]^{2-}$ at low temperature in DMF-d_7 results from two frozen C_{2h} and D_{2h} host–guest conformations, but interestingly, the conformational ratio C_{2h}/D_{2h} at T = 220 K depends significantly on the nature of the solvent. The C_{2h}/D_{2h} is about 5 : 1 in DMF-d_7 and 2 : 1 in CD_3CN.

$[Mo_{14}O_{14}S_{14}(OH)_{14}(H_2O)_3(C_9H_{14}O_4)]^{2-}$, $[Mo_{14}Azel]^{2-}$. The ^{1}H NMR spectrum of $(NMe_4)_2[Mo_{14}Azel]$ in D_2O consists of two broad signals centred at −0.38 and −0.68 ppm, corresponding to the $Azel^{2-}$ anion coordinated inside the molybdenum ring. Variable temperature experiments were then carried out in CD_3CN between 230 K and 320 K (see Fig. 6). At low temperature, 230 K, four NMR sharp lines ($\Delta\nu_{1/2}$ = 2–4 Hz) assigned to hydroxo bridges are observed at 9.71, 9.48, 8.91 and 8.44 ppm with integration 2 : 1 : 2 : 2, in agreement with C_{2v} symmetry. As the temperature increases, the hydroxo resonances significantly broaden and shift to low energies, as a result of the joint effects of solvation and fast proton exchange. Nevertheless, the signals corresponding to the methylene groups appear quite unaffected, in agreement with no dynamics for this system.

^{1}H DOSY NMR experiments

Diffusion NMR techniques have proved effective for the characterization of biological or supramolecular systems in solution, ion pairing or hydration rates.[29,32–36] The diffusion coefficient D_x of the cyclic oxothiomolybdenum, is experimentally determined with respect to an internal reference r, the $[Mo_{12}Trim]^{3-}$ ion (MM_r = 2139 g mol^{-1}, for non-solvated complex). The D_r/D_x ratio of the diffusion coefficients could be expressed according to eqn (2) within the framework of the Einstein–Smoluchowski–Stokes diffusion theory, as a function of the molecular weight MM_i (i = x or r) of the molecule in solution.[29,37,38]

$$\frac{D_r}{D_x} = 3\sqrt{\frac{MM_x}{MM_r}} \quad (2)$$

DOSY measurements were carried out on the ^{1}H signals of the alkyl chain encapsulated in $[Mo_{12}Adip]^{2-}$, $[Mo_{12}Pim]^{2-}$, $[Mo_{12}Sub]^{2-}$ and $[Mo_{14}Azel]^{2-}$. The protocol used for DOSY experiments is described in the Experimental section and the data (D_r/D_x ratios and molecular weights) are summarized in Table 3. Under non-exchange conditions in D_2O or in DMSO, the experimental molecular weights found for $[Mo_{12}Adip]^{2-}$, $[Mo_{12}Pim]^{2-}$, $[Mo_{12}Sub]^{2-}$ and $[Mo_{14}Azel]^{2-}$ are consistent with expectations, but values systematically lower by about 3–12% are observed for $[Mo_{12}Adip]^{2-}$, $[Mo_{12}Pim]^{2-}$, and $[Mo_{12}Sub]^{2-}$. Such slight differences could arise from solvation of the rings, experimentally evidenced by the solvent-dependence of the ^{1}H NMR chemical shifts of the hydroxo bridges and of the methylene groups in CD_3CN, DMF, and in DMSO (see Table 2). Systematic discrepancies could be related to the difference in solvation rate between the reference compound, *i.e.* the $[Mo_{12}Trim]^{3-}$ anion and the studied anion. Actually, an oxothiomolybdenum ring presents different potential sites for solvation, distributed as H-donor or H-acceptor. The water molecules bound from inside to the Mo atoms are sufficiently polarized to produce Brønsted acid sites acting as strong H-bond donors. Conversely, the hydroxo bridges can be either H-bond donors or acceptors. As previously shown for $[Mo_{12}Adip]^{2-}$, the first hydration sphere of the ring contains

Table 3 DOSY 1D ^{1}H NMR data obtained with various oxothiomolydenum wheels. $TerP^{2-}$, PDA^{2-} and $IsoP^{2-}$ ligands correspond to terphthalate, phenylene-diacetate and isophthalate ligands, respectively.[29]

Compound	Solvent	D_r/D_x found (expected)[a]	MM_x/g mol^{-1} found (expected)
$[Mo_{12}Adip]^{2-}$	D_2O	0.96 (0.99)	1892 (2076)
$[Mo_{12}Adip]^{2-}$	DMSO-d_6	0.98 (0.99)	2013 (2076)
$[Mo_{12}Pim]^{2-}$	DMSO-d_6	0.95 (0.99)	1830 (2090)
$[Mo_{12}Sub]^{2-}$	DMSO-d_6	0.96 (1.00)	1892 (2104)
$[Mo_{12}TerP]^{2-}$	D_2O	0.97 (0.99)[b]	1950 (2096)[b]
$[Mo_{12}TerP]^{2-}$	DMSO-d_6	0.96 (0.99)[b]	1910 (2096)[b]
$[Mo_{14}Azel]^{2-}$	D_2O	1.05 (1.05)	2480 (2494)
$[Mo_{16}(PDA)_2]^{4-}$	D_2O	1.17 (1.12)[b]	3430 (3032)[b]
$[Mo_{16}(IsoP)_2]^{4-}$	D_2O	1.14 (1.12)[b]	3180 (2997)[b]

[a] $[Mo_{12}Trim]^{3-}$ is used as an internal reference. [b] From ref. 29.

22 water molecules, symmetrically distributed over both sides of the ring. Such a *frozen* representation of the hydration sphere around the ring suggests that a comparable picture of the hydration process can be assumed in solution. The solvation rate of the ring should depend on several parameters, such as the charge density (for H-bond acceptor atoms), the presence of inner water molecules (H-bond donors), but also flexibility and dynamics of the ring in solution. It appears that solvation of the $[Mo_{12}Trim]^{3-}$ reference compound should also be taken into account. Then, the low molecular weight deduced from eqn (2) for compounds $[Mo_{12}Adip]^{2-}$, $[Mo_{12}Pim]^{2-}$, and $[Mo_{12}Sub]^{2-}$ in D_2O (or DMSO) could be assigned to a lower solvation rate of these compounds with respect to the reference. The difference in solvation rate could be estimated to be about 3–10 H_2O (or 0–3 DMSO) for the Mo_{12} ring systems (see Table 3). For $[Mo_{14}Azel]^{2-}$, the molecular weight obtained from eqn (2) is in good agreement with the expected value, meaning that the solvation rate could be similar to that of the $[Mo_{12}Trim]^{3-}$ reference. In this case, the lower charge of $[Mo_{14}Azel]^{2-}$ should be balanced by the presence of three inner water molecules, identified as strong H-bond donors. Conversely, the molecular weight of the large clusters $[Mo_{16}(PDA)_2]^{4-}$ and $[Mo_{16}(IsoP)_2]^{4-}$ are always overestimated,[29] in agreement with an increase of the solvation rate due to their higher ionic charges compared to $[Mo_{12}Trim]^{3-}$ and with the presence of polarized water molecules inside the ring.

Relative thermodynamic stabilities of $[Mo_{12}Adip]^{2-}$, $[Mo_{12}Pim]^{2-}$ and $[Mo_{12}Sub]^{2-}$ complexes

The three dicarboxylate anions adipate (C6), pimelate (C7) and suberate (C8) lead to dodecamolybdenum wheels. From such results, questions arise about the relative stability and the selectivity of the Mo_{12} ring with respect to these three guest molecules. To assess relative stabilities between $[Mo_{12}Adip]^{2-}$, $[Mo_{12}Pim]^{2-}$ and $[Mo_{12}Sub]^{2-}$ in water, the template-free precursor $K_{2-x}(NMe_4)_x[I_2Mo_{10}O_{10}S_{10}(OH)_{10}(H_2O)_5]$ was mixed at pH = 4.5 with two dicarboxylate ligands L1 and L2 with a ratio Mo_{12} : L1 : L2 corresponding to 1 : 1 : 1. The resulting spectra are presented in Fig. 7.

For the Mo_{12} : $Adip^{2-}$: L system with L = Pim^{2-} or Sub^{2-}, the resulting ^1H NMR spectra show the quasi-exclusive formation of $[Mo_{12}Adip]^{2-}$, whereas Sub^{2-} and Pim^{2-} remain free. These results indicate that $[Mo_{12}Adip]^{2-}$ is more stable than $[Mo_{12}Sub]^{2-}$ and $[Mo_{12}Pim]^{2-}$, which is associated with the selective encapsulation of the adipate anion. Unfortunately, accidental degeneracy of some resonances precludes the retrieval of more quantitative information but in the Mo_{12} : $Adip^{2-}$: Sub^{2-} or Mo_{12} : $Adip^{2-}$: Pim^{2-} mixtures, the $[Mo_{12}Adip]^{2-}$ anion represents more than 95% of the encapsulated species. The same protocol, using the components Mo_{12} : Pim^{2-} : Sub^{2-} leads to the preferential formation of the complex $[Mo_{12}Pim]^{2-}$ (around 85%) compared to $[Mo_{12}Sub]^{2-}$, indicating that the $[Mo_{12}Pim]^{2-}$ is more stable than $[Mo_{12}Sub]^{2-}$. The relative stabilities of the Mo_{12}-templated systems expressed as: $[Mo_{12}Adip]^{2-} > [Mo_{12}Pim]^{2-} > [Mo_{12}Sub]^{2-}$ therefore appear correlated with the length of the alkyl chains. The stability of a specific complex is then conditioned by the host–guest adaptability, which may be downgraded essentially by steric constraints affecting the alkyl chain within the Mo_{12} cavity. The X-ray structures (see Fig. 1), supported by DFT calculations

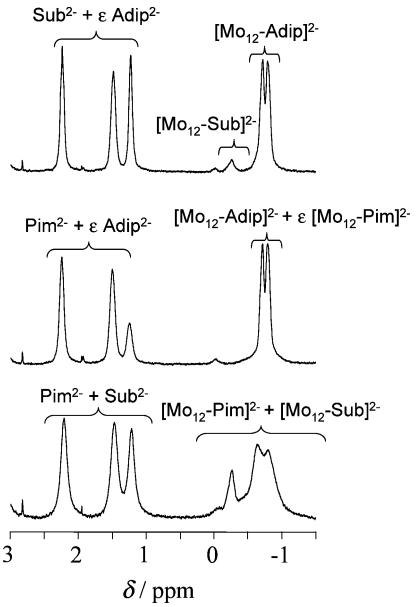

Fig. 7 300 MHz ^1H NMR spectra in D_2O of mixtures $Mo_{12}/Adip^{2-}/Sub^{2-}$ (top), $Mo_{12}/Adip^{2-}/Pim^{2-}$ (middle) and $Mo_{12}/Pim^{2-}/Sub^{2-}$ (bottom) in 1 : 1 : 1 ratio at pD around 4.9.

(see Fig. 8) reveal that the C6 alkyl chain of the adipate is quite relaxed and located in the mean plane of the 12 Mo atoms, while for the pimelate complex, the carbon chain is more constrained with an out-of-plane deviation of ~1.6 Å for the central carbon.[26] For the suberate anion, the severe disorder occurring within the alkyl chain precludes any experimental determination of geometrical parameters (bond distances and angles), but the geometric optimization carried out by DFT calculations reveals a folded chain, strongly displaced by about 2.1 Å out of the mean plane of the 12 Mo (see Fig. 8c).

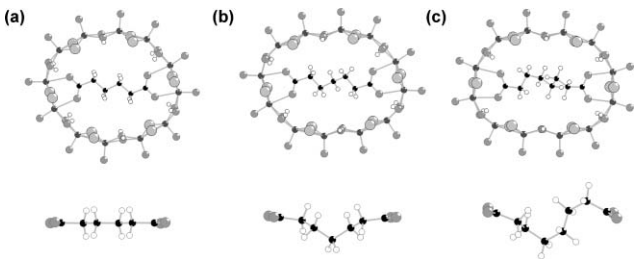

Fig. 8 DFT-optimized geometries of the complexes in the gas phase (top) with the corresponding side view of the isolated central dicarboxylate ion (bottom) for $[Mo_{12}Adip]^{2-}$ (a), $[Mo_{12}Pim]^{2-}$ (b) and $[Mo_{12}Sub]^{2-}$ (c).

DFT calculations

Computational strategy and results. DFT calculations and geometry optimizations have been carried out on host–guest complexes $[Mo_{12}Adip]^{2-}$, $[Mo_{12}Pim]^{2-}$ and $[Mo_{12}Sub]^{2-}$. Cyclic hosts with twelve molybdenum atoms have been considered and separately optimized assuming D_{6h} symmetry. Then, host–guest complexes have been considered with the dicarboxylate anions $Adip^{2-}$, Pim^{2-} and Sub^{2-} as guest molecules. All calculations have been carried out on molecules assumed isolated "in the gas phase". The crystal structure, slightly modified in some cases to

take advantage of the most probable symmetry, was taken as a starting point for geometry optimization, yielding the minimal energy of the complex, E_{min}(C). The most stable conformations obtained for $[Mo_{12}Adip]^{2-}$, $[Mo_{12}Pim]^{2-}$ and $[Mo_{12}Sub]^{2-}$ are depicted in Fig. 8. The structural models computed in the gas phase confirm the information obtained from X-ray diffraction and NMR studies. For $[Mo_{12}Adip]^{2-}$, although the water molecule has been omitted, the resulting structural model agrees well with the high symmetry observed by NMR in solution. In the case of $[Mo_{12}Pim]^{2-}$, the agreement between experimental and calculated molecular structures is excellent. Finally, the calculated structure for $[Mo_{12}Sub]^{2-}$ is also fully consistent with the experimental data obtained in the solid state (see Table 4 and S1, ESI‡).

After the optimization of the host–guest complex, separate single point (sp) calculations have been carried out on the host and on the guest fragments with the geometry optimized in the complex (E_{sp}(X, C) where X = host, or guest; and C refers to the considered host–guest complex), in order to assess the energy cost E_{adjust}(X, C) of their mutual adjustment to the host–guest structure (eqn 3). Note that E_{min}(X) represents the global energy minimum of fragment X:

$$E_{adjust}(X, C) = E_{sp}(X, C) - E_{min}(X) \quad (3)$$

The bonding energy $-\Delta E$(C) of the guest in the complex is then computed with respect to the sum of fragment energies:

$$\Delta E(C) = E_{min}(C) - E_{min}(host) - E_{min}(guest) \quad (4)$$

Note that the host molecule in the absence of carboxylate guests has been structurally characterized in a previous work.[39] The dodecamolybdate complex is indeed close to sixfold symmetry, but the cavity contains six water molecules, which are part of a more elaborate water cluster involving 16 molecules.[40] The formation of a host–guest complex with a dicarboxylate guest involves the displacement of this cluster. The true expression of ΔE(C) should take this process into account by removing the bonding energy of the water cluster within the molybdenum ring. Calculations are presently in progress to estimate this bonding energy, the order of magnitude of which should be ~80 kJ mol^{-1}.

For dicarboxylates exhibiting a linear alkyl chain, a large number of local energy minima are associated with the relative conformations of the methylene groups and with the concomitant folding of the carbon chain. The global minimum is systematically associated with an *all-trans* configuration of the chain, but the conformation computed with suberate and with pimelate guest molecules corresponds to a more compact folding associated with a local minimum, which is higher in energy. Table 5 reports the values of ΔE, E_{adjust}(host) and E_{adjust}(guest), together with the number N of local minima characterized for the free dianions. The relative energies E_{rel}(top) and E_{rel}(guest), which refer to the free dianions, are associated with the local minimum highest in energy, and with the equilibrium configuration topologically similar to that of the encapsulated ligand, respectively. The values of E_{rel}(top) and E_{rel}(guest) are computed with respect to the energy of the global minimum of the free anion. Note that E_{adjust}(guest) is always higher than E_{rel}(guest) because of local deformations not modifying the molecular topology. In aliphatic dicarboxylates the difference E_{adjust}(guest) − E_{rel}(guest) logically increases with the number of methylene groups.

Table 4 Computed interatomic distances (Å) compared to average experimental distances found in $[Mo_{12}Adip]^{2-}$, $[Mo_{12}Pim]^{2-}$ and $[Mo_{12}Sub]^{2-}$ anions

	Mo–O oxo	Mo–O hydroxo	O···O hydr-hydr	Mo–S	S···S	Mo–O carboxylate, H_2O	Mo···Mo opposite, short	Mo···Mo opposite, long	Mo···Mo
Mo_{12}, D_{6h}	1.693	2.112	2.342	2.341	3.639		12.28	12.28	2.843 × 6
									3.511 × 6
Suberate ⊂ Mo_{12}	1.70–1.71	2.09–2.17	2.30 × 2	2.33–2.37	3.64 × 4	2.39–2.41 × 4	10.37	13.51	2.84–2.85
			2.48 × 4		3.76 × 2	2.69, 2.85			3.38–3.47
Pimelate ⊂ Mo_{12}	1.70–1.71	2.09–2.16	2.30 × 2	2.33–2.37	3.65 × 4	2.40–2.41 × 4	10.36	13.75	2.83–2.85
			2.46 × 4		3.76 × 2	2.64 × 2			3.36 × 2
									3.48 × 4
Adipate ⊂ Mo_{12}	1.70–1.71	2.09–2.16	2.34 × 2	2.33–2.36	3.65 × 4	2.38–2.45 × 4	11.20	13.10	2.82–2.84
			2.46 × 4		3.76 × 2	2.87 × 2			3.39 × 2
									3.47 × 4
Average experimental distances	1.70	2.08	2.40	2.32	3.64	2.36	—	—	2.81
						2.47			3.31

Table 5 Host–guest complexes enclosing a dicarboxylate anion inside a $[Mo_{12}O_{12}S_{12}(OH)_{12}]$ cycle[a]

	ΔE[b]/kJ mol^{-1}	E_{adjust} (host)/kJ mol^{-1}	E_{adjust} (guest)/kJ mol^{-1}	N	E_{rel} (top)/kJ mol^{-1}	E_{rel} (guest)/kJ mol^{-1}
Adipate $\subset Mo_{12}$	−612.1	160.2	7.5	4	37.2	0.0
Pimelate $\subset Mo_{12}$	−569.4	164.8	36.0	12	46.0	28.0
Suberate $\subset Mo_{12}$	−543.9	163.6	43.9	25	43.1	22.2

[a] ΔE (host − guest bond energy), E_{adjust} (energy required for the structural adjustment of the host or of the guest), N (number of local minima characterized for the free dianion), E_{rel}(top) (relative energy of the highest local minimum of the free dianion), E_{rel}(guest) (relative energy of the local minimum of the free dianion associated with the observed configuration of the guest). [b] Calculated according to eqn (4). Solvation energy, and more specifically the bonding energy of the water cluster in $[Mo_{12}O_{12}S_{12}(OH)_{12}(H_2O)_6]$ have not been taken into account.

The adipate dianion is the only one for which the configuration of the carbon chain found in the complex is similar to the configuration of lowest energy for the uncoordinated molecule. The energy cost for structural adjustment is therefore very weak: 7.5 kJ mol^{-1}. For the longer carbon chains, the configuration observed in the complex is not amongst the most stable ones. The energy separating the local minimum from the global one amounts to 22–28 kJ mol^{-1}, and some additional energy is necessary for adjusting to the optimal guest structure in the complex (E_{adjust} = 36.0 kJ mol^{-1} for pimelate and 43.9 kJ mol^{-1} for suberate; Table 5). Preliminary calculations using the COSMO formalism[41] to take into account the solvent effects on the free dicarboxylate ions however indicate that the energy gaps are smaller among the local minima and with respect to the global minimum, thus reducing E_{rel} values.

The inclusion of the dicarboxylate guests induces an impressive deformation of the molybdenum ring, from circular to elliptical. However, the geometry optimization of a free dodecamolybdenum ring constrained to be elliptical yields an energy loss of 3.1 kJ mol^{-1} only, providing confirmation that the ring is flexible to a large extent and probably liable to coordination with various kinds of guest molecules. The values calculated for the energy cost of the host distortion induced by guest inclusion (E_{adjust}(host)) are however considerably higher (~160 kJ mol^{-1}, Table 5). This suggests that the adjustment energy mainly comes from *local* deformations induced by the coordination of the carboxylate groups. The nature of these local deformations can be assessed by a comparison between interatomic distances in the free dodecamolybdenum ring and in the various complexes (Table 4). They mainly affect the Mo–$O_{hydroxo}$ bond lengths, but also the shape and folding of the Mo_2O_2 and Mo_2S_2 metallacycles influenced by the complexation of the guest (Table 4, Fig. 8).

The complexation energy of the aliphatic carboxylates exhibits the expected increase with the rigidity of the carbon chain: $[Mo_{12}Adip]^{2-}$ > $[Mo_{12}Pim]^{2-}$ > $[Mo_{12}Sub]^{2-}$ (Table 5). Note however that the observed structure of $[Mo_{12}Adip]^{2-}$ involves a water molecule remaining inside the wheel, which was not considered in the present calculations. The major part of the computed energy differences can be assigned to the increase of E_{adjust}(guest) when more methylene groups are present (Table 5). The remaining differences could be attributed to slight changes in the strength of the secondary interactions between the carboxylate groups and *adjacent* Mo atoms: two such contacts are present in all three complexes, with Mo···O distances varying between 2.64 and 2.87 Å (Table 4). The probability of generating tenuous repulsive contacts between the alkyl chain and the host cage also increases with the size of the chain and the correlated elliptical deformation of the host wheel. Moreover, the carboxylate groups of the suberate guest tend to deviate from the mean plane of the metal atoms (Fig. 8c).

The crucial role of E_{adjust}(guest) in determining the relative stabilities of the three complexes with alkyl chains raises the question of assigning to the suberate or pimelate chains in the complex a configuration intrinsically more stable, but remaining compatible with the structure of the host. This latter condition rules out the configuration associated with the global minimum of both carboxylates, which is too much extended in space. A constraint was therefore assigned to the distance between carboxylate groups. Various conformations were obtained for suberate as for pimelate, but none of them was shown to exhibit a complexation energy lower than that deduced from the observed structures.

Conclusion

Interestingly, the use of the C6 (adipate), C7 (pimelate) and C8 (suberate) di-anions does not change the nuclearity of the inorganic ring, which remains fixed to Mo_{12}, whereas an increase of the alkyl chain from C8 to C9 (azelaate anion) leads to the formation of a Mo_{14} ring. Three new host–guest complexes, namely $[Mo_{12}Adip]^{2-}$, $[Mo_{12}Sub]^{2-}$ and $[Mo_{14}Azel]^{2-}$ self-assembled around adipate, suberate and azelaate anions have been synthesized and structurally characterized in the solid state and in solution. The $[Mo_{14}Azel]^{2-}$ anion is the only tetradeca-oxothiomolybdenum wheel and the largest member of the series ranging from Mo_8- to Mo_{14}-ring clusters self-assembled around saturated linear dicarboxylate ligands.

The NMR and X-ray results demonstrate that the oxothiomolybdenum rings are solvated in solution either with H_2O or with aprotic solvents such as DMF of DMSO. Investigations of the relative stabilities in the series of Mo_{12} rings encapsulating $Adip^{2-}$, Pim^{2-} and Sub^{2-} highlight the adaptability of the guest within a constant perimeter lined by the 12 Mo atoms. The stability of the host–guest systems decrease as the length of the alkyl chain increases, because the constraints affecting the alkyl chain concomitantly increase.

DFT calculations bring a crucial support to the experimental results. They confirm that host–guest adaptability is not equivalent across the Mo_{12} series and proved the inorganic ring to be highly flexible (about 3.1 kJ mol^{-1} from unconstrained circular to elliptical conformation). The major differences concerning complexation energies originate in the distortion of the alkyl chain, which determines the scale of stability between the three molybdenum wheels.

Experimental

Physical methods

Water content was determined by thermal gravimetric analysis (tga7, Perkin-Elmer). Infrared spectra were recorded on a Magna 550 Nicolet spectrophotometer, using KBr pellets. NMR measurements were performed on a Bruker Avance 300 or a Bruker avance 400 spectrometer, operating at 300 MHz or at 400 MHz, respectively, in 5 mm tubes. Chemical shifts were referenced to the external TMS standard. Diffusion experiments were recorded at 400 MHz-proton-Larmor frequency at room temperature in D_2O or in DMSO-d^6. The sequence corresponds to Bruker pulse program *ledpgp2s*[42] using stimulated echo, bipolar gradients and longitudinal eddy current delay as *z* filter. The four 2 ms gradients pulses have sine-bell shapes and amplitudes ranging linearly from 2.5 to 50 G cm^{-1} in 32 steps. The diffusion delay was 100 ms and the number of scans 16 or more. The processing was done using a line broadening of 5 Hz and the diffusion rates D_x calculated using the Bruker processing package, by analysing the decay of the natural logarithm of the normalized signal intensity I/I_0 of selected NMR signals as a function of the square of the pulse gradient strength according to eqn (5)[33] (I is the observed intensity, I_0 is the intensity without gradients, γ is the gyromagnetic ratio of the observed nucleus, δ is the length of the gradient pulse, G is the gradient strength, Δ (diffusion delay) is the delay between the midpoints of the gradients).

$$\ln\left(\frac{I}{I_0}\right) = -(\gamma\delta)^2\left(\Delta - \frac{\delta}{3}\right)DG^2 \qquad (5)$$

The NMR tubes were prepared by dissolving in 750 μL of D_2O or DMSO an equimolar mixture of an "unknown" compound (x) with the reference sample (r) (*ca.* 5–10 mg of each compound). Finally, the mixtures Mo_{12}/L1/L2, where L1 and L2 are $Adip^{2-}$, Pim^{2-} or Sub^{2-} are prepared by mixing in D_2O (1 mL) the molybdenum precursor $K_{2-x}(NMe_4)_x[I_2Mo_{10}O_{10}S_{10}(OH)_{10}(H_2O)_5]\cdot 20H_2O$ and the required quantity of buffered solutions of L1 and L2 to obtain an Mo_{12}/L1/L2 mixture in 1 : 1 : 1 ratios at pH around 4.5 (pD = 4.9).

X-Ray crystallography

The single crystals of compounds $(NMe_4)_2[Mo_{12}Adip]$, $K_2[Mo_{12}Sub]$ and $(NMe_4)_2[Mo_{14}Azel]$ are air sensitive and were recorded in capillaries at 293 K or in paratone oil at 100 K. X-Ray intensity data were collected on a Bruker-Nonius X8-APEX2 CCD area-detector diffractometer using Mo-K_α radiation (λ = 0.71073 Å). Data reduction was accomplished using SAINT V7.03 (APEX2 version 1.0–8; Bruker AXS: Madison, WI, 2003). The substantial redundancy in data allowed a semi-empirical absorption correction (SADABS V2.10) to be applied, on the basis of multiple measurements of equivalent reflections. The structures were solved by direct methods, developed by successive difference Fourier syntheses, and refined by full-matrix least-squares on all F^2 data using SHELXTL V6.12 (SHELXTL version 6.12; Bruker AXS: Madison, WI, 2001). Dimensions of crystals and crystallographic data are reported in Table 1, whereas selected bond lengths are listed in Table S1.‡ For $(NMe_4)_2[Mo_{12}Adip]$ and $(NMe_4)_2[Mo_{14}Azel]$, hydrogen atoms were included in calculated positions and allowed to ride on their parent atoms, whereas they were not considered in $K_2[Mo_{12}Sub]$, in regard of the high disorder of the alkyl chain. Moreover, in the case of $K_2[Mo_{12}Sub]$, we can note that the potassium cations are found disordered with the lattice water molecules.

Computational details

DFT calculations have been carried out with the 2004 version of the ADF program[43–45] using the gradient-corrected BP86 exchange–correlation functional.[46,47] All atoms are described with the Slater basis sets referred to as TZP in the User's Guide. The basis set for hydrogen is triple zeta plus one p-type orbital. For non-metal atoms, the core (He for oxygen, Ne for sulfur) is frozen and described by a single Slater function, whereas the valence set is triple-zeta and supplemented with a d-type polarization function. The small core (3s3p3d) of molybdenum was also modelled by a frozen Slater basis. The valence shell is double zeta for 4s, triple zeta for 4p, 4d and 5s, and supplemented with a single Slater orbital describing the 5p shell.

Syntheses

The compounds $K_{2-x}(NMe_4)_x[I_2Mo_{10}O_{10}S_{10}(OH)_{10}(H_2O)_5]\cdot 20H_2O$ ($0 < x < 0.5$), $Rb_2[Mo_{12}Pim]$ and $K_3[Mo_{12}Trim]$ were prepared as previously described in the literature[26,29,48] and checked by routine methods. Adipic, pimelic and suberic acids were purchased from Aldrich Chemicals.

$(NMe_4)_2[Mo_{12}O_{12}S_{12}(OH)_{12}(H_2O)(C_6H_8O_4)]\cdot 24H_2O$, $(NMe_4)_2[Mo_{12}Adip]\cdot 24H_2O$. To 1 g of precursor $K_{2-x}(NMe_4)_x[I_2Mo_{10}O_{10}S_{10}(OH)_{10}(H_2O)_5]\cdot 20H_2O$ (*ca.* 0.42 mmol) in 50 mL of water is added a slight excess of adipic acid (75 mg, 0.51 mmol) in 70 mL of water. The pH is adjusted to 5 with KOH 1 M and the resulting orange solution is heated to 50 °C for 45 min before standing overnight at RT. A first precipitate is removed by filtration and 75 mg of NMe_4Cl (0.68 mmol) in water (10 mL) are added to the filtrate under stirring. The resulting mixture is centrifuged and the resulting clear solution is left to stand in air. After 1 d, orange hexagonal single crystals of $(NMe_4)_2[Mo_{12}Adip]$ (250 mg, 27%) are obtained, isolated by filtration, washed with water and dried in air. Elemental analysis found: C 6.30; H 3.62; N 1.06; S 14.72; Mo 42.85. Calc. for $(NMe_4)_2[Mo_{12}O_{12}S_{12}(OH)_{12}(H_2O)(C_6H_8O_4)]\cdot 24H_2O$ (M = 2675 g mol^{-1}): C 6.29; H 3.54; N 1.05; S 14.38; Mo 43.04%. TGA: loss of 24.6 H_2O between RT and 210 °C. IR/cm^{-1}: 1533(s), 1481(ms), 1413(m), 970(s), 935(s), 526(s). NMR ^1H (DMSO-d_6 (ppm)): 11.29 (s, 4H); 10.37 (s, 8H); 3.08 (s, 24 H, NMe_4^+); −0.65 (s, 4H); −1.17 (s, 4H). EDX atomic ratio found (calc.): Mo/S = 1.09 (1.00). No trace of K^+ or Na^+.

$Cs_2[Mo_{12}O_{12}S_{12}(OH)_{12}(H_2O)(C_6H_8O_4)]\cdot 7DMF\cdot 11H_2O$, $Cs_2[Mo_{12}Adip]\cdot 7DMF\cdot 11H_2O$. 80 mg of adipic acid (0.55 mmol) in 15 mL of DMF are added to 1 g of precursor $K_{2-x}(NMe_4)_x[I_2Mo_{10}O_{10}S_{10}(OH)_{10}(H_2O)_5]\cdot 20H_2O$ (*ca.* 0.42 mmol) in 15 mL of water. The pH is adjusted to 5 with NaOH 1 M and the resulting orange solution is heated to 50 °C for 45 min before adding an excess of CsCl (250 mg, 1.5 mmol) at RT. A first precipitate is removed by centrifugation and the orange filtrate is kept in air. After several days, air-sensitive orange crystals are obtained (240 mg, 23%), isolated by filtration,

washed with water and dried in air. Elemental analysis found: C 10.23; H 2.79; N 3.00; S 13.09; Mo 37.40; Cs 8.01. Calc. for $Cs_2[Mo_{12}O_{12}S_{12}(OH)_{12}(H_2O)(C_6H_8O_4)]\cdot 7DMF\cdot 11H_2O$ (M = 3069.9 g mol^{-1}): C 10.56; H 3.05; N 3.19; S 12.53; Mo 37.50; Cs 8.66. IR/cm^{-1}: 1534(s), 1492(mw), 1436(m, DMF), 1414(m), 1387(m, DMF), 1252(mw, DMF), 1105(ms, DMF), 970(s), 935(s), 543(s). NMR ^{1}H (DMSO-d_6 (ppm)) : 11.30 (s, 4H); 10.39 (s, 8H); 7.95 (s, *ca* 7H, DMF); 2.89 (s, *ca* 21 H, DMF); 2.73 (s, *ca* 21 H, DMF); −0.65 (s, 4H); −1.16 (s, 4H). NMR ^{1}H (D_2O (ppm)): 7.82 (s, *ca*. 7H, DMF); 2.90 (s, *ca*. 21 H, DMF); 2.75 (s, *ca*. 21 H, DMF); −0.71 and −0.79 (two overlapping singlets, 8 H). EDX atomic ratio found (calc.): Mo/S = 1.09 (1.00); Mo/Cs = 5.90 (6.00).

$Rb_2[Mo_{12}O_{12}S_{12}(OH)_{12}(H_2O)(C_6H_8O_4)]\cdot 11H_2O$, $Rb_2[Mo_{12}Adip]\cdot 11H_2O$. To 1 g of precursor $K_{2-x}(NMe_4)_x[I_2Mo_{10}O_{10}S_{10}(OH)_{10}(H_2O)_5]\cdot 20H_2O$ (*ca*. 0.42 mmol) in water (30 mL) are added 80 mg of adipic acid (0.55 mmol) in water (10 mL) and 1.1 mL of 1 M potassium hydroxide. The pH of the resulting orange solution is about 5.0. The mixture is heated at 50 °C for 45 min. A first precipitate is removed by filtration and 300 mg of RbCl (2.48 mmol) are added to the filtrate. After a second filtration, the new filtrate is kept in air. After several days hexagonal orange crystal of $(NMe_4)_2[Mo_{12}Adip]$ are formed and removed again. Several days later, big orange crystals are obtained, isolated by filtration, washed with cold water and dried in vaccum. TGA: loss of *ca*. 11 H_2O between RT and 200 °C. IR/cm^{-1}: 1607(s), 1522(s), 1411(s), 964(s), 935(s), 524(s). NMR ^{1}H (DMSO-d_6 (ppm)) : 11.29 (s, 4H); 10.37 (s, 8H); −0.65 (s, 4H); −1.16 (s, 4H). EDX atomic ratio found (calc.): Mo/S = 1.04 (1.00); Mo/Rb = 5.83 (6.00).

$K_{1.8}(NMe_4)_{0.2}[Mo_{12}O_{12}S_{12}(OH)_{12}(H_2O)(C_8H_{12}O_4)]\cdot 22H_2O$, $K_2[Mo_{12}Sub]\cdot 22H_2O$. To 60 mg of suberic acid (0.34 mmol) deprotonated twice by molar KOH in water (20 mL), is added 1 g of precursor $K_{2-x}(NMe_4)_x[I_2Mo_{10}O_{10}S_{10}(OH)_{10}(H_2O)_5]$ (*ca*. 0.42 mmol). The pH is adjusted to 5 with 1 M KOH or HCl solutions. The resulting orange solution is heated to 50 °C for 45 min. The mixture is centrifuged and the obtained orange solution is left to slowly evaporate in air. After a week, orange crystals are obtained (600 mg, 83%), isolated by filtration, washed with water and dried in air. The following analyses are in agreement with a mixture of single crystals of $K_2[Mo_{12}Sub]$ with a minor proportion of $(NMe_4)_2[Mo_{12}Sub]$ complex. Elemental analysis found: C 4.20; H 3.00; S 14.88 14.13; Mo 44.71; K 2.77. Calc. for $K_{1.8}(NMe_4)_{0.2}[Mo_{12}O_{12}S_{12}(OH)_{12}(H_2O)(C_8H_{12}O_4)]\cdot 22H_2O$ (M = 2585.9 g mol^{-1}): C 4.09; H 2.74; S 14.88; Mo 44.52; K 2.72%. TGA: loss of *ca*. 22 H_2O between RT and 210 °C. IR/cm^{-1}: 1540(s), 1523(s), 1480(sh, w), 1414(ms), 971(s), 526(s). NMR ^{1}H (DMSO-d_6 (ppm)): 11.21 (s, 4H); 10.23 (s, 8H); 3.08 (s, 2.4 H : NMe_4^+); −0.5 to −1.2 (m, 12H). EDX atomic ratio found (calc.): Mo/S = 1.05 (1.00); Mo/K = 6.14 (6.66), S/K = 5.82 (6.66).

$Cs_2[Mo_{12}O_{12}S_{12}(OH)_{12}(H_2O)(C_8H_{12}O_4)]\cdot 4DMF\cdot 13H_2O$, $Cs_2[Mo_{12}Sub]\cdot 4DMF\cdot 13H_2O$. 90 mg of suberic acid (0.52 mmol) in DMF (15 mL) are added to 1 g of precursor $K_{2-x}(NMe_4)_x[I_2Mo_{10}O_{10}S_{10}(OH)_{10}(H_2O)_5]\cdot 20H_2O$ (0.42 mmol) in water (15 mL). The pH is adjusted to 5 with 1 M hydrochloric acid and the resulting orange solution is heated to 50 °C for 45 min before adding a slight excess of CsCl (250 mg, 1.5 mmol) at RT. A first precipitate is removed by centrifugation and the orange filtrate is kept in air. After 1 d, air-sensitive orange crystals are obtained (490 mg, 56%), isolated by filtration, washed with water and dried in air. Elemental analysis found: C 8.10; H 2.56; N 2.15; S 13.64; Mo 39.07. Calc. for $Cs_2[Mo_{12}O_{12}S_{12}(OH)_{12}(H_2O)(C_8H_{12}O_4)]\cdot 4DMF\cdot 13H_2O$ (M = 2497.3 g mol^{-1}): C 8.29; H 2.71; N 1.93; S 13.28; Mo 39.74%. IR/cm^{-1}: 1532(s), 1492(w, DMF), 1436(m, DMF), 1414(m), 1384(s), 1252(m, DMF), 1105(ms, DMF), 967(s), 926(s), 543(s). NMR ^{1}H (DMSO-d_6 (ppm)): 11.22 (s, 4H); 10.23 (s, 8H); 3.06 (s, 24 H: NMe_4^+); −0.5 to −1.2 (m, 12H). EDX atomic ratio found (calc.): Mo/S = 1.11 (1.00); Mo/Cs = 6.58 (6.00), S/Cs = 5.91 (6.00).

$(NMe_4)_2[Mo_{14}O_{14}S_{14}(OH)_{14}(H_2O)_3(C_9H_{14}O_4)]\cdot 24H_2O$, $(NMe_4)_2[Mo_{14}Azel]\cdot 24H_2O$. To 1 g of precursor $K_{2-x}(NMe_4)_x[I_2Mo_{10}O_{10}S_{10}(OH)_{10}(H_2O)_5]\cdot 20H_2O$ (*ca*. 0.42 mmol) in water (10 mL) are added azelaic acid (57 mg, 0.27 mmol) in water (10 mL) and 0.56 mL of 1 M potassium hydroxide solution. The pH is adjusted to 4.5 and the resulting orange solution is warmed at 50 °C for 20 min. A crude yellow precipitate is removed by centrifugation and a small amount of NMe_4Cl (30 mg, 0.1 mmol) is added to the filtrate. After several days, orange hexagonal crystals are obtained (180 mg, 21%), isolated by filtration, washed by water and dried in air. Elemental analysis found: C 6.57; H 3.74; N 0.97; S 14.99; Mo 43.62. Calc. for $(NMe_4)_2[Mo_{14}O_{14}S_{14}(OH)_{14}(H_2O)_3(C_9H_{14}O_4)]\cdot 24H_2O$: C 6.64; H 3.47; N 0.91; S 14.60; Mo 43.69%. TGA: loss of 27 H_2O between RT and 200 °C. IR/cm^{-1} (KBr pellet): 1539(s), 1481(ms), 1437(mw), 1419(mw) 959(s), 508(s). NMR ^{1}H (D_2O (ppm)): 3.06 (s, 24 H, NMe_4^+); −0.38 (s, 8H); −0.68 (s, 6H). EDX atomic ratio calcd. (found): Mo/S = 1.00 (1.00). No trace of K^+.

Acknowledgements

S.F. and J.-F.L. are grateful to Virginie Blanchet and Vincent Girlando for their contribution to the experimental work. DFT calculations have been carried out at the CINES Computer Centre (Montpellier, France) and at the CURRI centre (ULP, Strasbourg, France).

References

1 N. Mizuno, S. Hikichi, K. Yamaguchia, S. Uchida, Y. Nakagawa, K. Uehara and K. Kamata, *Catal. Today*, 2006, **117**, 32–36.
2 N. Mizuno and M. Misono, *Chem. Rev.*, 1998, **98**, 199–217.
3 M. Bonchio, M. Carraro, A. Sartorel, G. Scorrano and U. Kortz, *J. Mol. Catal. A: Chem.*, 2006, **251**, 93–99.
4 R. Neumann and A. M. Khenkin, *Chem. Commun.*, 2006, 2529–2538.
5 H. Yanagie, A. Ogata, S. Mitsui, T. Hisa, T. Yamase and M. Eriguchi, *Biomed. Pharmacother.*, 2006, **60**, 349–352.
6 S. Mitsui, A. Ogata, H. Yanagie, H. Kasano, T. Hisa, T. Yamase and M. Eriguchi, *Biomed. Pharmacother.*, 2006, **60**, 353–358.
7 J. T. Rhule, C. L. Hill and D. A. Judd, *Chem. Rev.*, 1998, **98**, 327–357.
8 P. Mialane, C. Duboc, J. Marrot, E. Riviere, A. Dolbecq and F. Sécheresse, *Chem.–Eur. J.*, 2006, **12**, 1950–1959.
9 P. Mialane, A. Dolbecq and F. Sécheresse, *Chem. Commun.*, 2006, 3477–3485.
10 J. M. Clemente-Juan and E. Coronado, *Coord. Chem. Rev.*, 1999, **195**, 361–394.
11 E. Coronado and C. J. Gomez-Garcia, *Chem. Rev.*, 1998, **98**, 273–296.
12 A. Müller, F. Peters, M. T. Pope and D. Gatteschi, *Chem. Rev.*, 1998, **98**, 239–271.
13 D. E. Katsoulis, *Chem. Rev.*, 1998, **98**, 359–387.
14 A. Müller, F. Peters, M. T. Pope and D. Gatteschi, *Chem. Rev.*, 1998, **98**, 239–271.

15 G. Liu, T. B. Liu, S. S. Mal and U. Kortz, *J. Am. Chem. Soc.*, 2006, **128**, 10103–10110.
16 U. Kortz, F. Hussain and M. Reicke, *Angew. Chem., Int. Ed.*, 2005, **44**, 3773–3777.
17 A. Müller, Y. S. Zhou, H. Bogge, M. Schmidtmann, T. Mitra, E. T. K. Haupt and A. Berkle, *Angew. Chem., Int. Ed.*, 2006, **45**, 460–465.
18 A. Müller, P. Kogerler and A. W. M. Dress, *Coord. Chem. Rev.*, 2001, **222**, 193–218.
19 E. Cadot, M.-A. Pilette, J. Marrot and F. Sécheresse, *Angew. Chem., Int. Ed.*, 2003, **42**, 2173–2176.
20 P. Kogerler and L. Cronin, *Angew. Chem., Int. Ed.*, 2005, **44**, 844–846.
21 D. L. Long, E. Burkholder and L. Cronin, *Chem. Soc. Rev.*, 2007, **36**, 105–121.
22 E. Cadot and F. Sécheresse, *Chem. Commun.*, 2002, 2189–2197.
23 F. Sécheresse, A. Dolbecq, P. Mialane and E. Cadot, *C. R. Chim.*, 2005, **8**, 1927–1938.
24 E. Cadot, M. J. Pouet, C. R. Robert-Labarre, C. du Peloux, J. Marrot and F. Sécheresse, *J. Am. Chem. Soc.*, 2004, **126**, 9127–9134.
25 E. Cadot, B. Salignac, J. Marrot and F. Sécheresse, *Inorg. Chim. Acta*, 2003, **350**, 414–420.
26 B. Salignac, S. Riedel, A. Dolbecq, F. Sécheresse and E. Cadot, *J. Am. Chem. Soc.*, 2000, **122**, 10381–10389.
27 S. Floquet, J. Marrot and E. Cadot, *C. R. Chim.*, 2005, **8**, 1067–1075.
28 A. Dolbecq, C. du Peloux, A. L. Auberty, S. A. Mason, P. Barboux, J. Marrot, E. Cadot and F. Sécheresse, *Chem.–Eur. J.*, 2002, **8**, 350–356.
29 J.-F. Lemonnier, S. Floquet, J. Marrot, E. Terazzi, C. Piguet, P. Lesot, A. Pinto and E. Cadot, *Chem.–Eur. J.*, 2007, **13**, 3548–3557.
30 A. Dolbecq, E. Cadot and F. Sécheresse, *C. R. Acad. Sci., Ser. IIc: Chim.*, 2000, **3**, 193–197.
31 E. Cadot, J. Marrot and F. Sécheresse, *Angew. Chem., Int. Ed.*, 2001, **40**, 774–777.
32 L. Allouche, A. Marquis and J. M. Lehn, *Chem.–Eur. J.*, 2006, **12**, 7520–7525.
33 E. Martinez-Viviente, P. S. Pregosin, L. Vial, C. Herse and J. Lacour, *Chem.–Eur. J.*, 2004, **10**, 2912–2918.
34 I. Fernandez, E. Martinez-Viviente and P. S. Pregosin, *Inorg. Chem.*, 2005, **44**, 5509–5513.
35 E. Terazzi, S. Torelli, G. Bernadinelli, J. P. Rivera, J.-M. Bénech, C. Bourgogne, B. Donnio, D. Guillon, D. Imbert, J.-C. G. Bünzli, A. Pinto, D. Jeannerat and C. Piguet, *J. Am. Chem. Soc.*, 2005, **127**, 888–903.
36 M. Greenwald, D. Wessely, I. Golberg and Y. Cohen, *New J. Chem.*, 1999, **23**, 337–344.
37 M. Pons and O. Millet, *Prog. Nucl. Magn. Reson. Spectrosc.*, 2001, **38**, 267–324.
38 C. S. Johnson, Jr., *Prog. Nucl. Magn. Reson. Spectrosc.*, 1999, **34**, 203–256.
39 E. Cadot, B. Salignac, S. Halut and F. Sécheresse, *Angew. Chem., Int. Ed.*, 1998, **37**, 611–612.
40 The central hexamer is organized as a planar, ring-shaped water cluster involving six intra-cluster hydrogen bonds and a complex network of hydrogen bonds with the two $(H_2O)_5$ clusters located above and below the ring cavity.
41 A. Klamt and G. Schüürmann, *J. Chem. Soc., Perkin Trans. 2*, 1993, 799–805.
42 D. H. Wu, A. D. Chen and C. S. Johnson, Jr., *J. Magn. Reson., Ser. A*, 1995, **115**, 260–264.
43 G. Te Velde, F. M. Bickelhaupt, E. J. Baerends, C. Fonseca Guerra, S. J. A. van Gisbergen, J. G. Snijders and T. Ziegler, *Comput. Chem.*, 2001, **22**, 931–967.
44 C. Fonseca Guerra, J. G. Snijders, G. Te Velde and E. J. Baerends, *Theor. Chem. Acc.*, 1998, **99**, 391–403.
45 *ADF2004.01*, SCM/Vrije Universiteit, Theoretical Chemistry, Amsterdam, The Netherlands, 2004, http://www.scm.com.
46 A. D. Becke, *J. Chem. Phys.*, 1993, **98**, 5648–5652.
47 J. P. Perdew, *Phys. Rev. B*, 1986, **B33**, 8822–8824.
48 E. Cadot, B. Salignac, J. Marrot, A. Dolbecq and F. Sécheresse, *Chem. Commun.*, 2000, 261–262.

